Received: 6 February 2023 | Revised: 15 April 2023 | Accepted: 17 April 2023

DOI: 10.1002/pol.20230072

RESEARCH ARTICLE

JOURNAL OF POLYMER SCIENCE WILEY

In-situ study of degradation in PTB7:PCBM films prepared with the binary solvent additive DPE:DIO

Dominik M. Schwaiger[1] | **Wiebke Lohstroh**[2] | **Marcell Wolf**[2] | **Christopher J. Garvey**[2] | **Peter Müller-Buschbaum**[1,2]

[1]Department of Physics, Chair for Functional Materials, TUM School of Natural Sciences, Technical University of Munich, Garching, Germany

[2]Heinz Maier-Leibnitz Zentrum (MLZ), Technical University of Munich, Garching, Germany

Correspondence
Peter Müller-Buschbaum, Department of Physics, Chair for Functional Materials, TUM School of Natural Sciences, Technical University of Munich, James-Franck-Str. 1, Garching 85748, Germany.
Email: muellerb@ph.tum.de

Funding information
German Federal Ministry of Education and Research, Grant/Award Number: 05K16WO3; Deutsche Forschungsgemeinschaft, Grant/Award Number: EXC 2089/1 – 390776260

Abstract

Blend films of poly[[4,8-bis[(2-ethylhexyl)oxy]benzo[1,2-b:4,5-b′]dithiophene-2,6-diyl][3-fluoro-2-[(2-ethylhexyl)carbonyl]thieno[3,4-b]thiophenediyl]] (PTB7) in combination with 6,6-phenyl-C61-butyric-acid-methyl-ester (PCBM) are a model system for low bandgap organic photovoltaics. Typically, solvent additives are used to improve the power conversion efficiencies of the resulting devices but possibly also decrease the device stability. In this study, we use the binary solvent additive 1,8-diiodooctane:diphenylether (DIO:DPE) for PTB7:PCBM blend films and study how different film drying procedures influence the physical and chemical stability of the polymer blend. The strong influence of the drying procedure on the stability against photoinduced degradation of the PTB7:PCBM films, produced with solvent additives, is shown with data from UV–visible (UV–vis), Fourier transform infrared (FTIR) and Raman spectroscopy. The addition of solvent additive molecules DIO:DPE to the PTB7:PCBM blend accelerates the degradation compared with the pristine blend. At higher annealing temperature a removal of the additives is bringing degradation back to the level of the pristine blend films, which is promising for photovoltaic applications.

KEYWORDS

bulk heterojunction, degradation, organic photovoltaics, solvent additive, spectroscopy

1 | INTRODUCTION

On the road toward marketability, organic photovoltaics (OPVs) have made impressive progress in recent years.[1–3] OPVs especially create interest due to their versatility as the starting materials can be molecularly engineered in combination with devices produced from solution in thin film architecture or on flexible substrates. The wet chemical approach offers possibilities for a cheap large scale production by using coating methods such as slot die coating[4–7] or spray deposition,[8,9] to bridge the gap between lab scale and commercial application.[10,11] Today, power conversion efficiencies (PCEs) have already exceeded 19%,[12–18] which implies that organic solar cells (OSCs) are ready to become commercially prevalent against conventional silicon solar cells that have dominated the photovoltaic (PV) market for three decades. Nonetheless, there are challenges preventing the breakthrough of the emergent PV technologies. One major concern is that some of the materials used in OPVs are

significantly affected by physical and chemical degradation when exposed to ambient atmosphere and illumination. This is problematic for a profitable long-term operation of PV devices.[19–25] Degradation is largely a problem of the active layer, where photons are absorbed, excitons are created, subsequently split, and free charges are transported toward the electrodes. Because the separation of excitons requires a material interface, the active layer is generally composed of at least two materials with different electronic properties, an electron donor and an electron acceptor, which are typically arranged in a bulk heterojunction (BHJ) architecture.[26–32]

Besides work on newly developed donor and acceptor materials, over the years different classes of model systems have been established in the field. Typically, their PCE values stay behind the recent record setting systems, however, their value is related in the existing large body of literature knowledge. In such a scenario, it is possible to gain further in-depth knowledge. For the class of fullerene derivate based OPVs, PCBM for many years was the dominating acceptor material. In combination with the conjugated polymer PTB7 as electron donor, PTB7:PCBM developed as low bandgap model system.[33–35] Figure 1 shows the chemical formulae of the two major components PTB7 and PCBM. The subunits of the polymer PTB7 are indicated as TT (thienothiophene) and BDT (benzodithiophene) units.

In the present work, we expand the knowledge of the system PTB7:PCBM concerning degradation, by studying the influence of a binary solvent additive on the stability of the PTB7:PCBM blend in ambient conditions and illumination.[36–41] Over the years, solvent additives have been proven to facilitate the desired microstructure in the active layer due to their selective solubility, thereby improving the PCE significantly.[42–48] The addition of 3% DIO and 2% DPE to the casting solution was reported to be a good combination for increasing the PCE of PTB7:PCBM based devices from below 7% (without solvent additive) to 9.25%.[49] The use of solvent additives requires

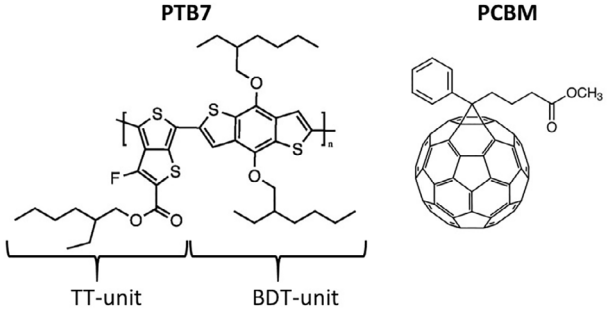

FIGURE 1 Chemical structures of the polymer PTB7 and the fullerene molecule PCBM.

an adequate adaption of the drying procedure since their boiling points are generally higher (168 °C for DIO, 259 °C for DPE) compared to the bulk solvent chlorobenzene (132 °C). In particular, an incomplete removal of solvent additive can lead to even more unstable active layers and open additional degradation pathways beyond the material's intrinsic physical and chemical degradation mechanisms.[44,50–54]

In this study, the influence of the binary solvent additive DIO:DPE (3:2 vol%) dried by different protocols on the light-induced degradation of PTB7:PCBM blend films in ambient conditions is investigated. As reported before, the combined influence of irradiation and oxidizing agents such as O_2 and possibly solvent additive molecules is needed for the creation of reactive species and the alteration of the π-conjugated network in the process of photooxidation.[55–57] During exposure of the PTB7:PCBM blend samples to the two mentioned stimuli, ultraviolet–visible (UV–vis) absorption spectroscopy is used to determine the availability of electronic transitions and vibrational spectroscopy is selected to gain information about chemical bonding inside the samples. We show that the addition of solvent additive molecules to the polymer:fullerene blend leads to a rapid degradation of the resulting layer. We conclude that if the beneficial effects from the use of solvent additives are desired, a complete removal of these additives is absolutely critical to avoid serious degradation compared to films without solvent additives.

2 | RESULTS AND DISCUSSION

2.1 | Structure characterization

The (semi-) crystalline polymer stacking structure is probed with XRD. For the solvent additive free samples (Figure 2A) three weak and broad scattering features are found at 2-theta values of 9, 22, and 26° besides the major broad peak at 18.5°. This 2-theta value corresponds to a d-spacing of 4.8 Å, which can be interpreted as the stacking distance of the Π-Π system of the polymer.[58,59] In the sample that is produced with DIO:DPE as binary solvent additive (Figure 2B) the main diffraction peak is shifted to 19.5° and only one additional weak scattering feature is detectable at 23°. The shift of the main Bragg peak (and also of the smaller peak at 22°) by 1° toward higher angles indicates a contraction of the respective structure. The average Π-Π stacking distance in the solvent additive sample is calculated to be 4.6 Å. The loss of some of the Bragg peaks upon the use of DIO and DPE as solvent additives indicates a more uniform microstructure that is characterized by smaller crystalline domain sizes. This is suggested by the increase of the FWHM of the main

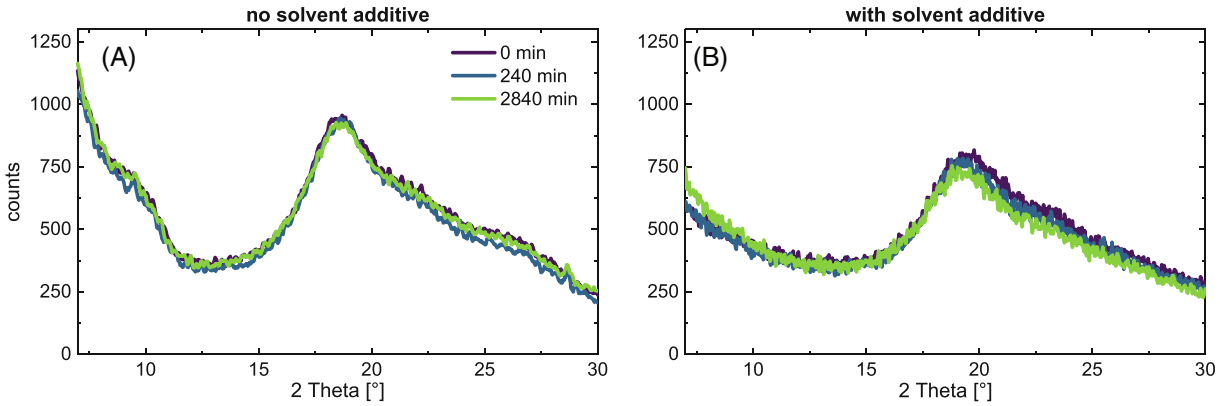

FIGURE 2 X-ray diffractograms of PTB7:PCBM films produced with (A) and without (B) solvent additive, both dried at 150 °C. Fresh samples (violet) are compared with illuminated samples (240 min in blue; 2840 min in green).

reflex. None of the XRD patterns is significantly affected by the illumination in ambient atmosphere. Hence, the light induced degradation mechanisms seem to only affect the local chemical structure, and not the (semi-) crystalline polymer stacking structure.

2.2 | Optical absorbance

In order to follow the evolution of the conjugation state and possible electronic transitions, UV–visible spectra are acquired after predetermined times of illumination. Figure 3 shows the comparison of the pristine films produced without and with the binary solvent additive. The absorbance curves are normalized to the first peak from the right at around 685 nm.

The use of DIO and DPE as solvent additives leads to a better defined absorption maximum between 600 and 700 nm comprised of two peaks. The film that is produced without solvent additive does also show the same absorption peaks, but the absorbance stays rather constant toward smaller wavelengths. When directly comparing the non-normalized spectra, acquired from films of similar thickness, it appears that the use of solvent additives rather increases the absorbance in the range between 600 and 700 nm, than decreases it in the lower wavelength region (see Figure S1 in the Supporting Information). As both, DIO and DPE have their absorption features at significantly lower wavelengths, the change in the UV–vis spectra can be attributed to a modification of the PTB7:PCBM blend structure.

When the pristine films are subjected to illumination under the presence of oxygen, as in the regular atmosphere (ambient conditions), they are expected to undergo chemical and physical degradation. This has been shown before for PTB:PCBM bulk heterojunctions as well as for similar systems.[38,57,60,61] For a fast, intense

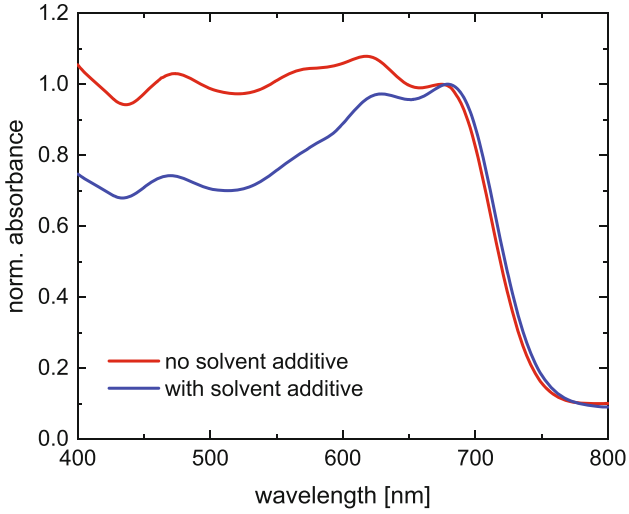

FIGURE 3 UV–vis absorbance spectra of PTB7:PCBM thin films drop cast from CB-solution with (blue) and without (red) DIO:DPE binary solvent additive. Absorbance values are normalized to the peak at around 680 nm.

degradation of the samples, these studies suggest the necessity of both, the presence of oxygen and the photon energy. In order to exclude a spontaneous occurrence of the expected degradation processes for the present samples, a set of films was prepared with and without solvent additives that was stored in the dark at ambient atmosphere. Repeated UV–vis measurements showed no sign of degradation in the absence of illumination as evident in Figure S2. Figure 4 shows the development of the UV–vis spectra during illumination of the film with a blue LED. From Figure 4, it becomes obvious that in case of the solvent additive prepared films, degradation, as probed by the optical absorbance, strongly depends on the initial drying temperature. No such effect is observed for the films prepared without solvent additive.

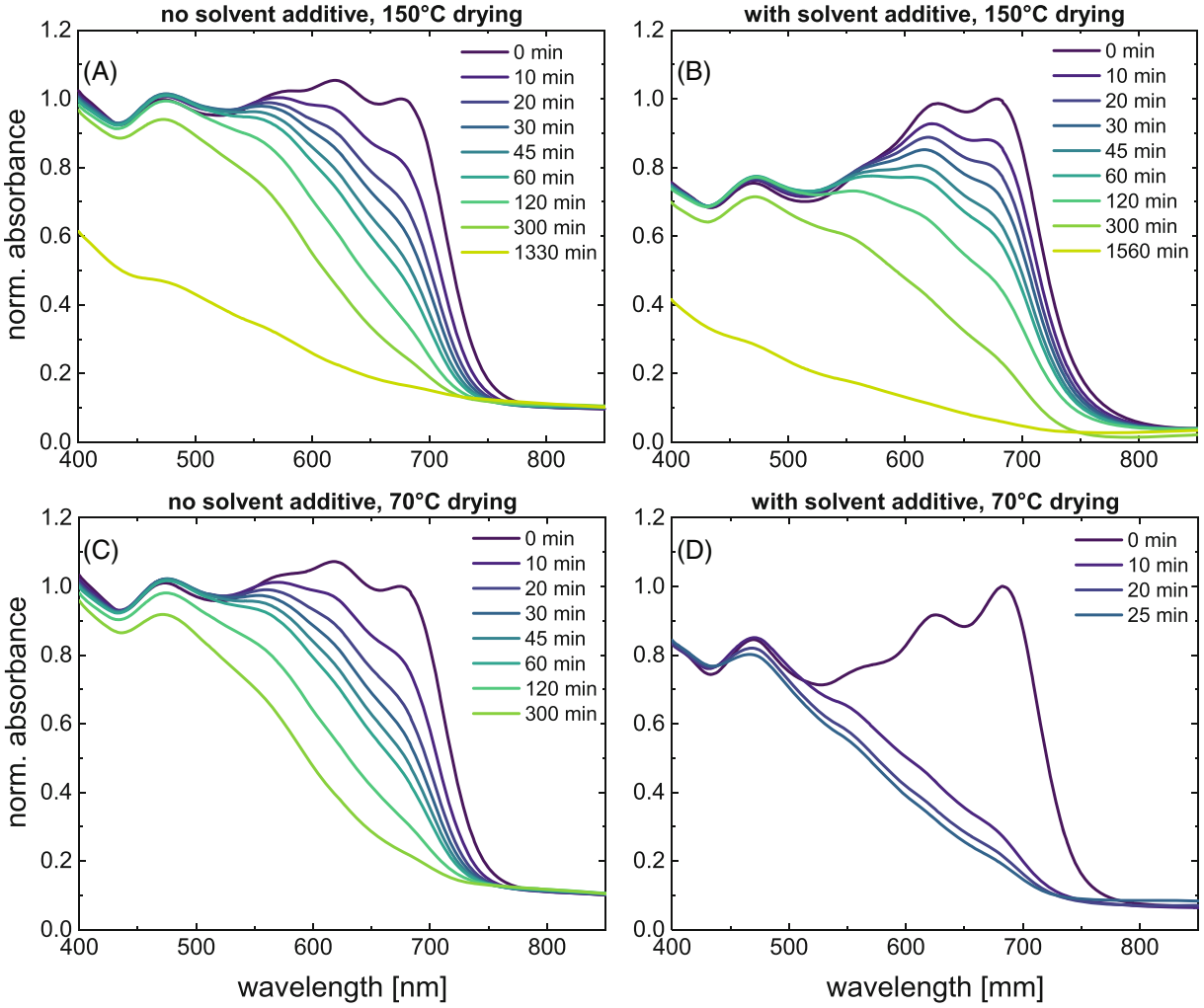

FIGURE 4 In-situ UV–vis absorbance spectra under illumination for PTB7:PCBM thin films produced with (B, D) and without (A, C) solvent additive at high (A, B) and low temperature (C, D) for the film drying. Each data set is normalized to the initial (0 min) spectrum's peak at around 680 nm.

For comparison this experiment is performed also with different LED light sources (blue, red and white). The experiment configuration, in particular the LED-sample-distance is determined in a way that the incident energy dose per unit area on the sample is the same for every light source. Information about the respective LEDs is given in the Supporting Information and UV–vis spectra showing the light induced loss of absorbance are both presented in Figure S3. In agreement with Löhrer and coworkers, who investigated the influence of incident light color on the photo-degradation in the system PTB7-Th:PCBM in greater detail, we find that blue, red and white LED illumination leads to a qualitatively similar degradation effect, as long as the incident radiation energy is kept constant.[60] Nonetheless, the color of the incident light can influence the specific loss of absorption in certain wavelength ranges. This behavior is shown in Figure 5 exemplarily for a sample produced without solvent additive, which displays the loss of absorbance in the spectral ranges around the red and blue LED's central wavelength for illumination with all three LEDs. Figure 5A indicates no clear influence of LED color on the loss of absorbance in the wavelength range between 430 and 530 nm (blue), whereas in Figure 5B, which shows the wavelength range from 580 to 680 nm (red) a clear dependence is evident. In this wavelength regime, the blue LED causes the slowest photo-degradation. As soon as the light source has a significant portion of red light, the photo-degradation happens considerably faster. This trend is shown by the black symbols in Figure 5 that stand for illumination with the white LED. The red LED, which naturally yields even a higher red light fraction, causes the strongest absorbance fade, even though only slightly stronger than the white LED. Since the incident energy is the same for all LEDs these findings show that the photo-degradation is caused by all LEDs over the entire spectrum but the presence of red light particularly accelerates this process in the corresponding wavelength

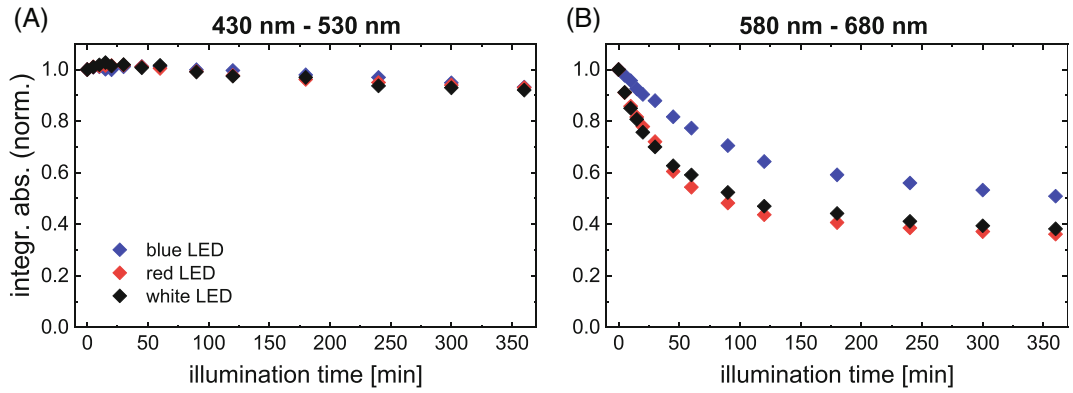

FIGURE 5 Integrated optical absorbance of a simple PTB7:PCBM blend film in the wavelength ranges 430 to 530 nm (A) and 580 to 680 nm (B). Values are normalized to the absorbance at $t = 0$ min. Blue symbols represent degradation caused by the blue LED, red symbols stand for the red LED and black symbols for the white LED.

range. An influence of LED color in the low wavelength range is not found. These findings show that the studied degradation is more dependent on the light intensity than the LED's central wavelength, at least in the visible range. For better comparability and the simplification for the measurement setups only the blue LED is used in the further degradation experiments.

Figure 4A,B display the absorption spectra of the completely dried films (at 150 °C) without and with solvent additives, respectively. All spectra rapidly lose absorbance in the two characteristic peaks at 625 and 683 nm within the first 2 h of (blue) LED illumination. These peaks originate from the polymer's conjugated network.[62] The low wavelength tail of the spectra is relatively insensitive to the light exposure and only is affected at very long illumination times. After 2 h most of the characteristic absorbance of the films is lost and a global bleaching over the entire wavelength range is apparent. This process continues over days to reduce the sample's absorbance. When films are dried at 70 °C, the film that is produced without solvent additive (Figure 4C) behaves roughly identically to the film that is dried at higher temperatures (Figure 4A). The comparison of the samples with solvent additives (Figure 4B,D) reveals a clear difference in the response to illumination over time. Whereas the properly dried film (Figure 4B) shows a relatively slow, gradual decrease of the characteristic absorbance, this process occurs on a shorter timescale when the drying temperature is reduced to 70 °C. Figure 4D illustrates an almost immediate loss of the absorption between 550 and 750 nm after 10 min of illumination.

To determine optical transitions of PTB7 and follow their evolution over the illumination time UV–vis spectra are fitted with Gaussian functions with equal width at half maximum height and distance between each other.[24,63,64] A detailed description of the fit procedure is found in the Supporting Information. In the following only the 0–0 and 0–1 transitions, represented by the first two Gaussian peaks, are analyzed, because higher transitions smear due to a high disorder in both, the physical and electronic structure of the materials.

Resulting peak integrals and positions of the 0–0 and 0–1 transitions are presented in Figure 6 as function of the illumination time. The area of a transition is proportional to the probability for it to occur. Figure 6A,B show a monotonous decay of probability of both transitions in all samples with increasing illumination time. This decrease is more distinct for the 0–0 transition (Figure 6A) than for the 0–1 transition (Figure 6B). Such behavior coincides with the impression from Figure 4, where the loss of absorbance is particularly pronounced in the high wavelength region. Comparing the behavior of the individual samples, both transitions show a similar picture. The solvent additive sample dried at low temperature (blue symbols) shows a decrease in the transition's probability almost immediately. The decay occurs much more slowly and gradually for the other two samples (red and black symbols). However, it should be noted that the high temperature dried solvent additive sample (red) shows a significantly higher stability for both transitions than the sample, produced without solvent additives. This finding might be explained with the intrinsically different absorbance spectrum of the samples in the wavelength range between 600 and 730 nm (compare Figure 4) originating from the structure modification, which is induced by the use of DIO:DPE as binary solvent additive.[49] As shown in Figure 6C,D, the specific energy of the 0–0 and 0–1 transition increases slightly with ongoing film degradation. While this shift is around 0.03–0.04 eV for the solvent additive free and high temperature dried sample with DIO:DPE (black and red symbols), its magnitude is almost doubled for the solvent additive sample dried at low temperature (blue symbols). This highlights the unstable structure of this sample.

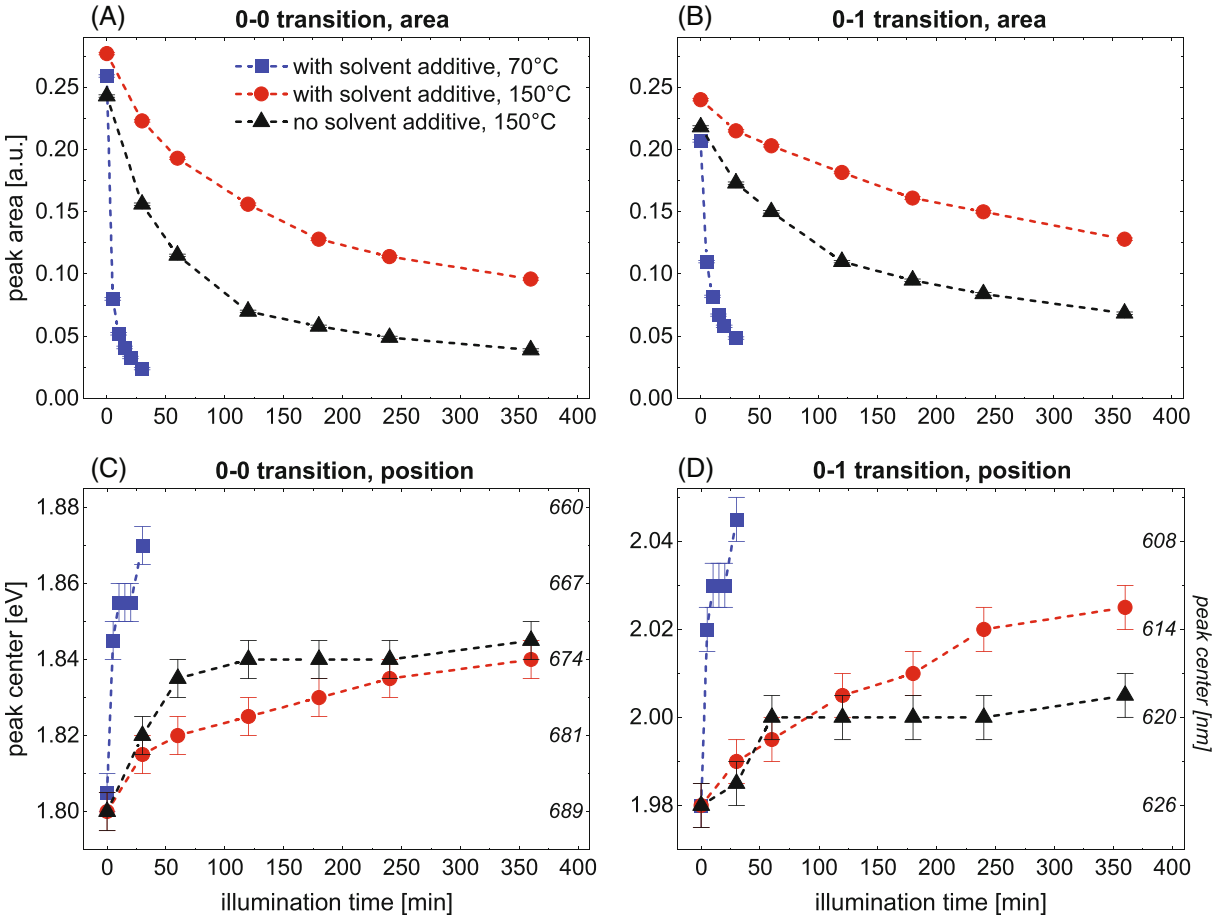

FIGURE 6 Results from in-situ UV–vis spectroscopy. UV–vis absorbance spectra are fitted with Gaussian functions to determine optical transitions of PTB7. (A) and (B) show the resulting area for the 0–0 and 0–1 transition, respectively, over illumination time. (C) and (D) show the corresponding position of the transitions in terms of energy. The dashed lines are a guide to the eye only.

Since a complete removal of the bulk solvent can be inferred from the data (see next section), the change in properties can most likely be attributed to residual solvent additive molecules. Even though the initial film shows comparable optical properties, it is much more unstable and loses its characteristic absorbance much faster than the completely dried film. Since no distinct difference between the different drying protocols is visible for the solvent additive free sample in the following only the 150 °C dried samples will be studied as reference.

2.3 | Changes in the chemical bonding

Fourier transform infrared spectroscopy is used to recognize chemical changes in the bonding structure of IR active functional groups with special focus on the polymer's conjugated system. Figure 7 shows an overview of the FTIR spectra in the relevant frequency ranges between 3000 and 2800 cm^{-1} as well as between 1800 and 1000 cm^{-1}. More precisely, films produced with and without DIO and DPE as binary solvent additive, and both, freshly prepared films and in a light-degraded state are compared. The dark blue lines are spectra of pristine films and the green lines are the FTIR spectra of the degraded films. No characteristic peaks of the solvents are visible, which indicates that the polymer:fullerene film is represented by the spectra. It is obvious that some absorbance peaks in the spectra are strongly attenuated, or completely erased upon illumination, whereas others remain constant and there are even parts in the spectra, that gain absorbance.

The assignment of the most prominent peaks is given by Table 1 in accordance to previous studies on comparable systems.[39,50,60,65] In the wavenumber range between 3000 and 2800 cm^{-1} we observe several peaks originating from CH_2 and CH_3 stretching modes of alkyl side chains. A slight decrease in the absorbance of these peaks can be observed in the film that is produced without solvent additive. This decrease is more pronounced in the solvent additive sample. Peaks in the region between 1800 and 1600 cm^{-1} are assigned to C═O

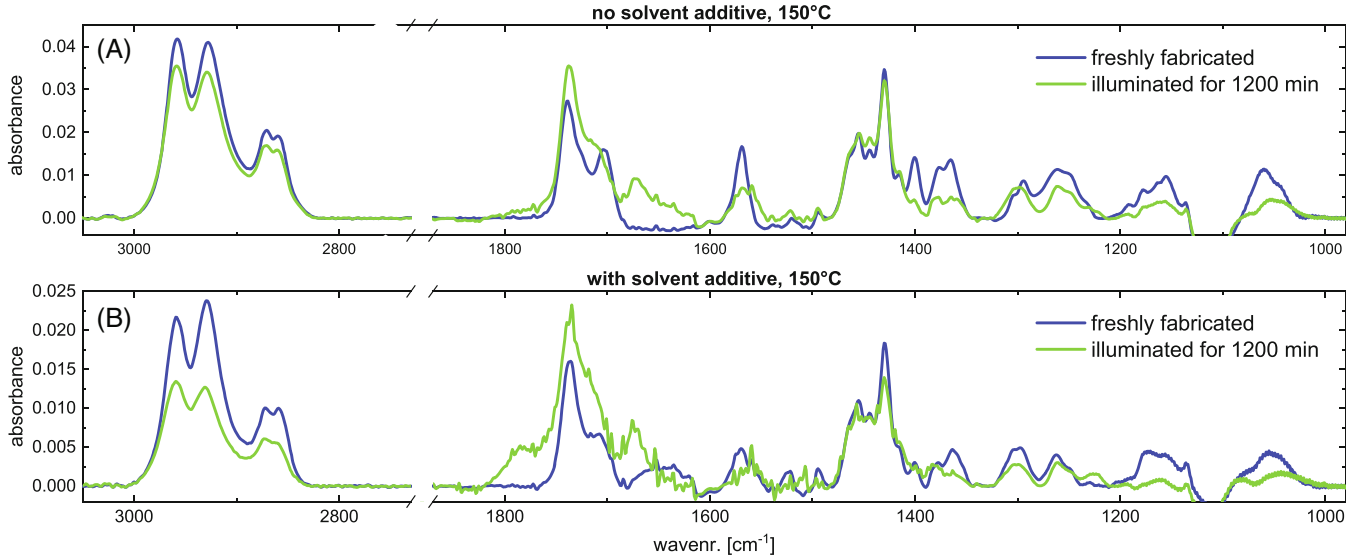

FIGURE 7 FTIR absorbance spectra of PTB7:PCBM thin film samples produced without (A) and with (B) solvent additive, both dried at 150 °C, around the relevant ranges from 3000 to 2800 cm^{-1} and 1800 to 1000 cm^{-1}, respectively. Dark blue curves are recorded for freshly prepared samples, whereas green curves show measurements of light and oxygen degraded samples.

stretching modes. The freshly fabricated films feature two distinct peaks at 1738 and 1705 cm^{-1}, respectively for C═O stretching modes of ester side chains. These peaks are sharper for the additive-free sample. The TT-related peak at 1705 cm^{-1} appears more distinct. These absorbance peaks are not increasing upon illumination but it seems that they get superimposed by adjacent broader peaks. This effect is more pronounced in the sample that is produced with solvent additives. The general increase of absorbance is attributed to the uptake of oxygen and the formation of new C═O bonds as one aspect of the light induced degradation process.[60] The peak that is found at 1570 cm^{-1} is attributed to C═C stretching modes in the thiophene rings of the thienothiophene segments. Toward lower wavenumbers, there are broad absorption bands between 1480 and 1420 cm^{-1} attributed to C—H bending modes. A characteristic peak at 1430 cm^{-1} reflects the stretching vibration in the benzene rings of PCBM. At 1400 cm^{-1} a sharp peak is present in the spectra of the pristine films. It almost vanishes in the degraded samples. This peak is assigned to the C—F stretching mode. It has to be noted, that this bond is present only once per PTB7 monomer.

Figure 8 displays the detailed spectral evolution in the relevant regions of the FTIR spectra (3000 to 2800 cm^{-1} and 1700 to 1350 cm^{-1}) over time, up to an illumination time of up to 1200 min: sample with solvent additives dried at 60 °C (Figure 8A,B); sample also with solvent additives dried at 150 °C (Figure 8C,D); and sample that is produced without solvent additive (Figure 8E,F).

TABLE 1 Peak positions of the most prominent IR absorption features with the assigned types of vibrations that are expected from the sample according to literature.[39,50,60,66]

Peak position	Assigned bond vibration
3000–2800 cm^{-1}	CH_2/CH_3 stretch in alkyl side chains
1800–1620 cm^{-1}	newly created C═O stretch
1738, 1705 cm^{-1}	C═O stretch in ester groups of PCBM & TT side chain
1569 cm^{-1}	C═C stretch in TT-thiophene rings
1490 cm^{-1}	C═C stretch in BDT-thiophene rings (weak)
1480–1420 cm^{-1}	CH_2/CH_3 bend, C═C stretch
1430 cm^{-1}	char. C═C stretch in PCBM benzene rings (const.)
1400 cm^{-1}	C—F stretch (TT)

Figure 8A,C,E compare the C—H stretching modes of the alkyl side chains. The well dried solvent additive sample and the neat polymer:fullerene blend sample behave almost identically. They feature the same peaks at identical positions and ratios. Over the entire displayed frequency range they lose about 15% absorbance uniformly. Figure 8A exhibits a completely different trend for the insufficiently dried sample with DPE:DIO. The freshly prepared film shows significant differences in the spectrum as the sample is exposed to light over time. The higher frequency peaks of the respective double peaks are strongly suppressed and hardly visible. This means that CH_2 vibrations are nicely visible and their intensity

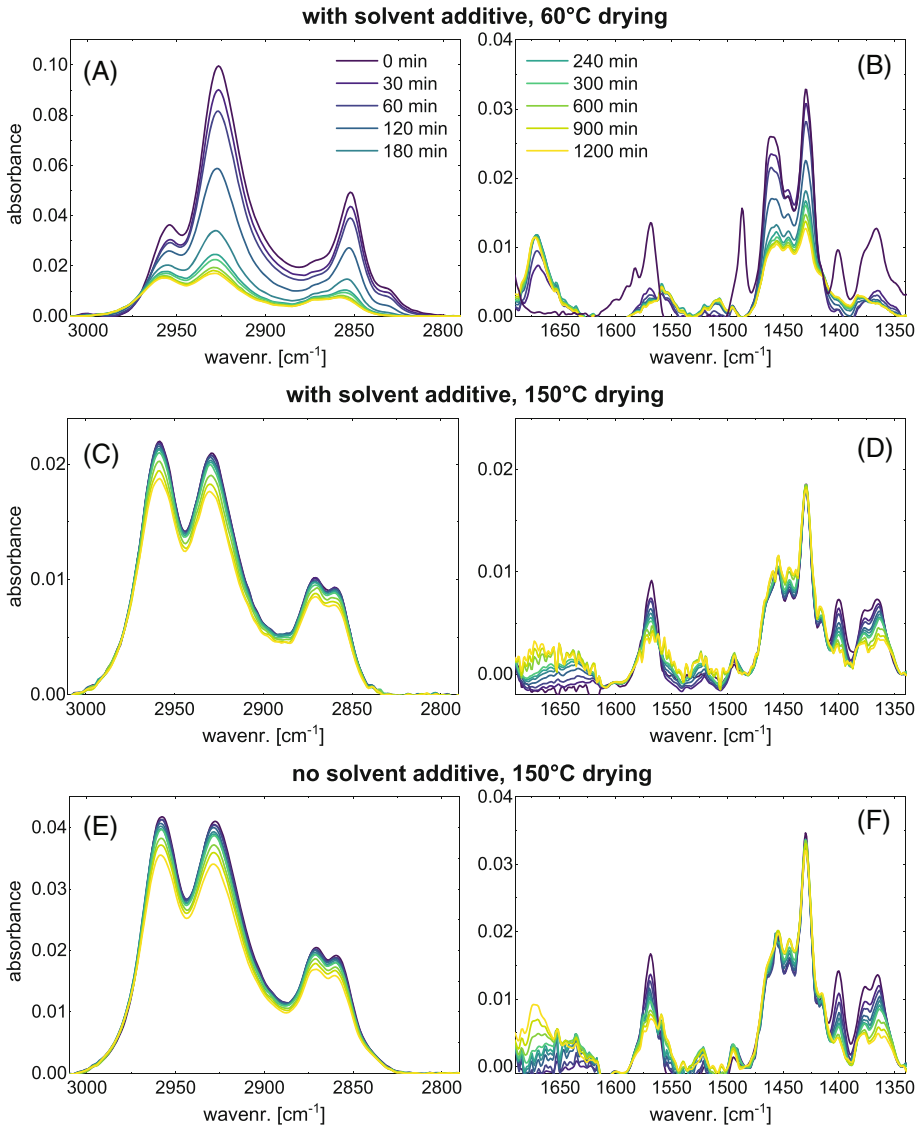

FIGURE 8 In-situ FTIR absorbance spectra of PTB7:PCBM thin films under LED illumination in the wavenumber ranges 3000 to 2800 cm^{-1} (A, C, E) and 1690 to 1350 cm^{-1} (B, D, F). From top to bottom the different samples with solvent additive dried at 60 °C (A, B), with solvent additive dried at 150 °C (C, D) and without solvent additive (E, F) are displayed.

and ratio match the other samples but the CH_3 vibrations cannot be observed, which might give a hint that residual solvent additive molecules could be located in the vicinity of the side chain ends and thus damp the CH_3 stretching vibrations.[50,60] The increase of sample transmission over time is faster for this sample compared to the other samples. 15% loss of absorbance, compared to the initial absorbance, is reached already within 48 min of illumination (extrapolated), whereas after the entire 1200 min there is a reduction of 83% in absorbance from the initial value.

The spectral region that is most relevant for the conjugated system of the polymer chain is shown in the right column of Figure 8B,D,F. The low temperature treated solvent additive sample shows by far the largest changes in the spectra with illumination time. The peaks at 1569, 1490, and 1400 cm^{-1} disappear completely almost immediately upon illumination. The band between 1480 and 1420 cm^{-1}, which is supposed to be relatively stable, significantly decreases in intensity, which indicates an accelerated degradation of PCBM. The high temperature dried solvent additive and the neat PTB7:PCBM sample, visible in Figure 8D,F, respectively, show a different behavior to the former and similar among each other. The peaks between 1480 and 1420 cm^{-1} remain constant in intensity, while the others decrease gradually to approximately half of the initial intensity. At wavenumbers around 1650 cm^{-1} a newly forming peak can be observed. It is assigned to photooxidation products associated with the thiophene system and indicates degradation induced formation of C═O bond stretching vibrations.[50,66] The spectra are fitted with a number of Lorentzian functions (see example in Figure S5) and integral intensities for selected peaks are plotted against illumination time in Figure 9. The violet, red and orange curves are representative for the alkyl side chains, blue

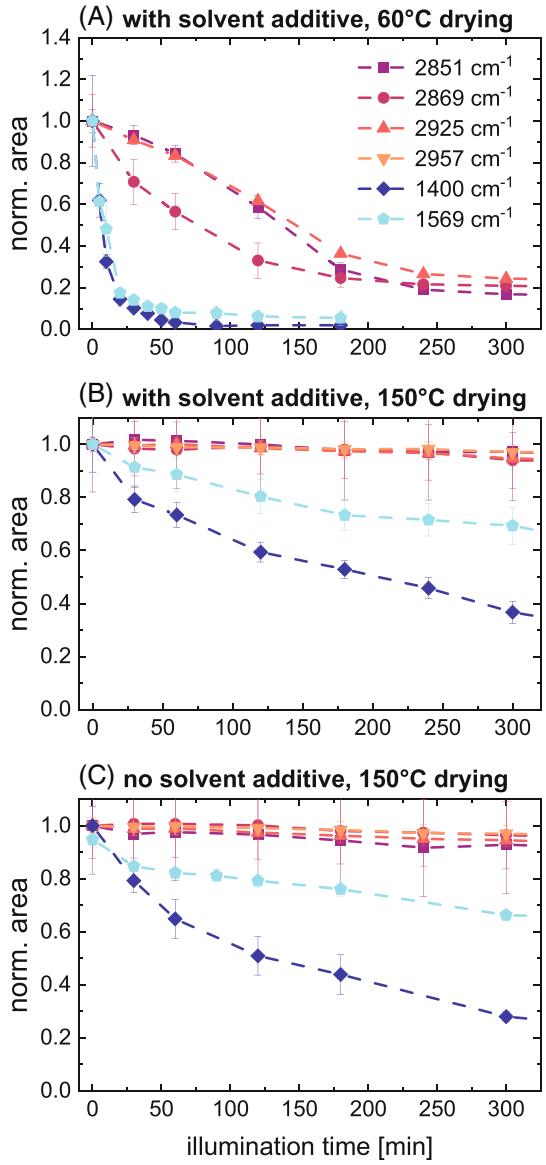

FIGURE 9 Development of intensities of selected IR absorption peaks in the CH_2/CH_3 (orange/red) and the characteristic C═C and C—F peaks (cyan/blue) from the fingerprint region. From top to bottom the different samples with solvent additive dried at 60 °C (A), with solvent additive dried at 150 °C (B) and without solvent additive (C) are displayed. A multiple Lorentzian fit was used and peak areas are normalized to $t = 0$ min.

and cyan stand for the characteristic C—F and C═C stretching modes in the thiophene rings of the conjugated system, respectively.

Generally, a decrease of the peak area can be observed, which indicates, that the respective functional groups are strongly affected by the degradation. The peak at 2957 cm^{-1} is excluded from the analysis due to its very low significance compared to the neighboring 2925 cm^{-1} peak, which is only 7% (see Figure 8A). A representative fit of the peak without deconvolving the influence of the rapidly changing neighbor peak was not possible. When comparing Figure 9B,C, there is only very little quantitative difference evident and they can be seen as qualitatively identical. This suggests that a drying temperature of 150 °C is sufficient to remove any DIO and DPE molecules or at least enables the formation of a film that is as stable as the one produced without solvent additives. On the other hand, the low temperature dried solvent additive sample (Figure 9A) shows a much more rapid decay of the characteristic IR absorbance peaks. The alkyl chain associated modes (except the 2957 cm^{-1} peak, already mentioned) loose between 70% and 80% in intensity, while they stay almost stable in the other two samples.

The peak, associated with the C—F stretching vibration at 1400 cm^{-1} decays for all samples, but while it diminishes by 80% almost immediately and completely vanishes after around 60 min in Figure 9A, the loss of intensity is much slower and more gradual in Figure 9B,C, where even after 300 min of illumination 30% to 40% of the initial peak area is left. A glance at the C═C bonds in the thiophene rings of the conjugated system yield very similar results for the low temperature dried solvent additive sample, as the absorbance of the 1569 cm^{-1} peak, visualized in cyan in Figure 9A drops very fast and disappears almost completely. For the high temperature dried solvent additive and solvent additive samples the decay is again much slower and 60% to 70% of the initial band intensity remain after 300 min illumination. Analogously to the results from optical absorption, the insufficient removal of solvent additive molecules results in a very unstable film, that is subjected to light and oxygen induced degradation in a much stronger way than the samples, which are dried at higher temperature or produced without solvent additive. As already reported before, the conjugated polymer backbone is affected more, compared to the alkyl side chains or fullerene domains.[39,40,65] The C—F bond stands out here with especially strong degradation susceptibility.

2.4 | Laser induced degradation followed by Raman spectroscopy

Besides the illumination induced degradation with LEDs, also laser light sources as used in spectroscopic studies can themselves induce degradation. Here we use a Raman laser (785 nm), which itself causes the degradation in the excitation spot for the measurements.[38,65] The observed kinetics enable an investigation of the development of the stacking structure of the conjugated polymer system. Raman scattering is used to follow primarily the C═C stretching vibrations. The FTIR and Raman

degradation studies are complementary to each other, since the degradation of the films is induced by different light sources characterized by different intensities and thus occurred on differing timescales. Due to the higher incident intensity per unit area of the laser, changes observed by Raman scattering are expected to occur faster.

The range of Raman shifts from 1100 to 1650 cm^{-1} contains the features, which are representative of the polymer's conjugated system. Figure 10 shows Raman spectra in this range during laser illumination time of 120 min. The assignment of the individual peaks is given in Table 2. Figure 10A depicts data from the low temperature dried sample with the binary DIO:DPE solvent additive, whereas Figure 10B,C are representative for the high temperature dried solvent additive and the neat blend sample, respectively. It is evident, that the signal of the solvent additive sample, dried at 60 °C is significantly noisier than the other two and, analogously to the observations from FTIR spectroscopy, peak intensity is dropping much more rapidly. These effects are unlikely to be caused by the changes in the surface morphology of the films as profilometry measurement shows no significant differences, especially for the two samples that are produced with solvent additives (see Figure S6). There is a very fast decay of peak intensity for the solvent additive sample dried at 60 °C. As it is also obvious in Figure 11A, the peak intensities drop below 30% of the initial value within the first 10 min of illumination, whereas they appear more stable in the other samples (Figure 11B,C).

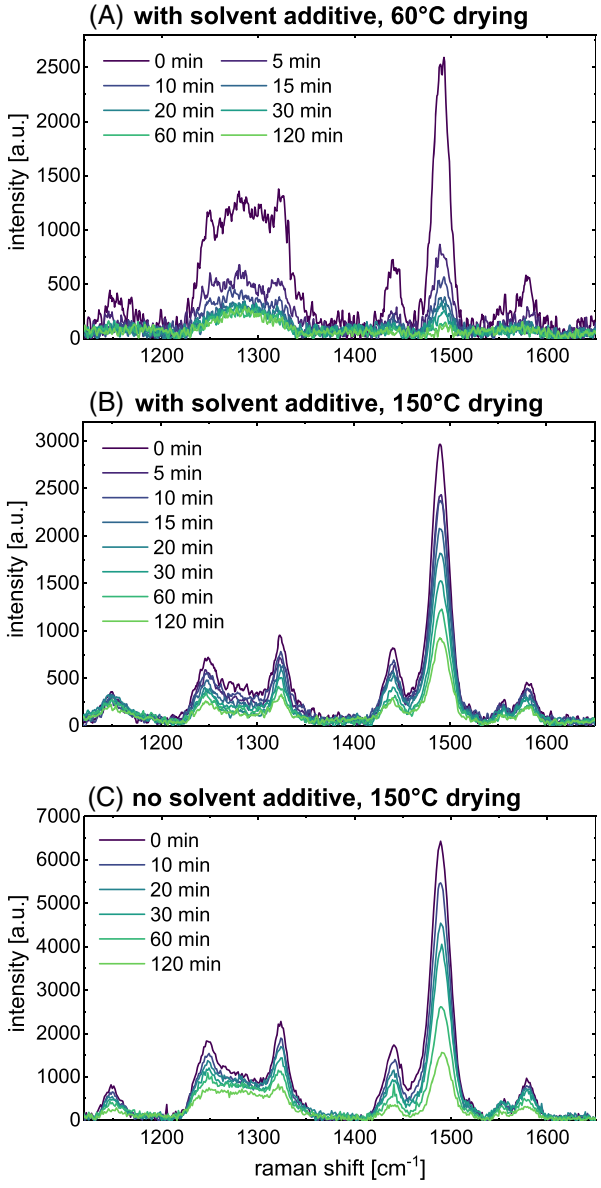

FIGURE 10 In-situ Raman spectra of PTB7:PCBM thin films under Laser (785 nm) illumination in the Raman shift range from 1120 to 1670 cm^{-1}. From top to bottom the different samples with solvent additive dried at 60 °C (A), with solvent additive dried at 150 °C (B) and without solvent additive (C) are displayed.

Of particular interest are the peaks between 1400 and 1600 cm^{-1} assigned to C═C double bonds in thiophene and benzene rings of PTB7 domains. The variation of the peak intensities with time are shown in Figure 11 for all three samples for the first 60 min of illumination. It is apparent that in the well dried samples the peak at 1580 cm^{-1} is more stable over the illumination time compared to the other peaks. This finding indicates that the thienothiophene segments of the polymer chain are less affected than the benzodithiophene segments represented by the peaks at 1440 and 1490 cm^{-1}. While they lose about 50% of intensity, the 1580 cm^{-1} peak shrinks by only ~30% within the first 45 min of illumination. Two peaks, which describe C—H and C—C bonds in the side chains, are overlapping in a broad peak around 1300 cm^{-1}. In Figure 10A the broad peak remains stable, while the peaks that are discussed before vanish almost

TABLE 2 Peak positions of the most prominent Raman peaks with the assigned types of vibrations that are expected from the sample according to literature.[38,65,67]

Raman peak position	Assigned bond vibration
1250 cm^{-1}	C—H asymmetric bend
1325 cm^{-1}	C—C stretch
1440 cm^{-1}	C═C stretch in TT-thiophene rings & BDT backbone
1490 cm^{-1}	C═C stretch in BDT backbone & side chains
1550 cm^{-1}	C═C stretch in non-fluorinated TT-thiophene rings
1570 cm^{-1}	C═C stretch in fluorinated TT-thiophene rings

immediately. In Figure 10B,C, the peaks are more stable and decrease more gradually over time in a similar fashion. The broader feature seems to be relatively stable, but less distinct in the well dried solvent additive sample. This behavior may indicate that the broad feature around a Raman shift of 1280 cm^{-1} represents a structure, which can be attributed to the bonding of solvent molecules, rather than to the polymer:fullerene system. After reporting many similarities between the solvent additive sample, dried at 150 °C and the pure PTB7:PCBM sample, the results from Raman spectroscopy presented in Figure 10 show some differences for the two. The broad peak at 1280 cm^{-1} is almost stable in the solvent additive free sample (Figure 10C), whereas it decreases for the well dried solvent additive sample in the same way as most other peaks.

Figure 12 shows the evolution of the relative Raman peak intensities. All peak intensities are added and normalized to 100% for each measurement. The general trend for all samples is a decrease of the very prominent peak at 1490 cm^{-1} and a relative increase of the peaks that are located at lower Raman shifts. This indicates the denaturation of the conjugated system under

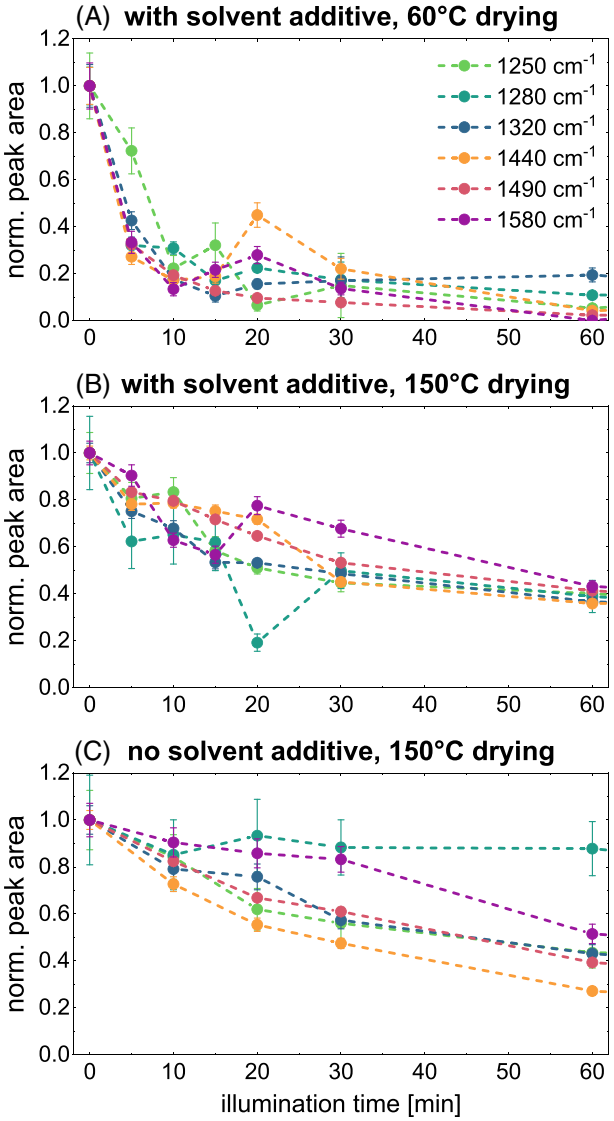

FIGURE 11 Development of intensities of selected Raman peaks. From top to bottom the different samples with solvent additive dried at 60 °C (A), with solvent additive dried at 150 °C (B) and without solvent additive (C) are displayed. A multiple Lorentzian fit is used and peak areas are normalized to $t = 0$ min. Dashed lines are guides to the eye.

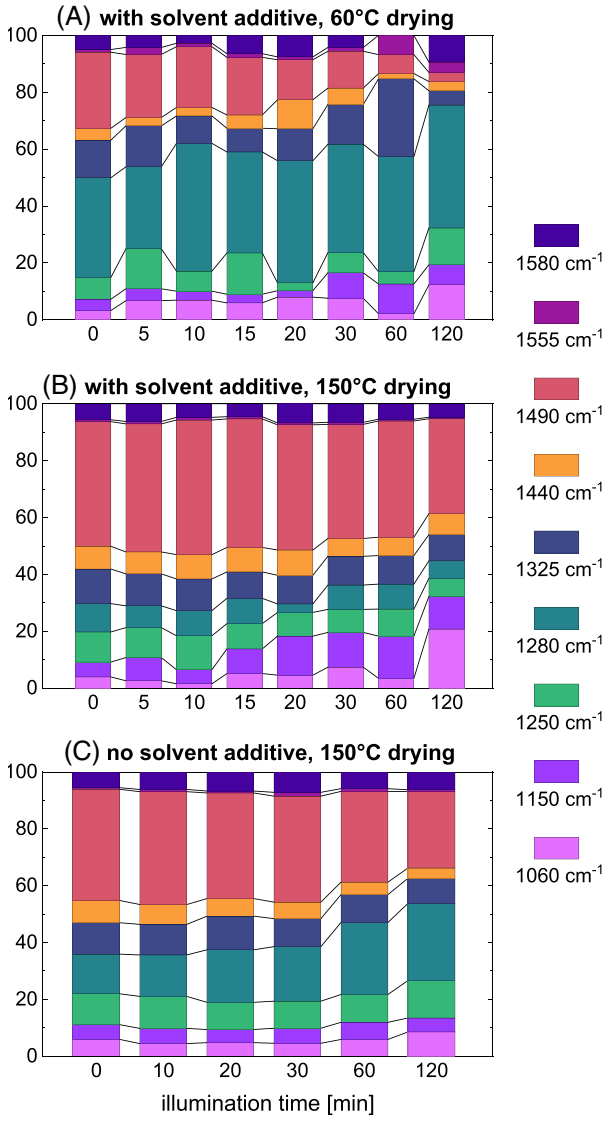

FIGURE 12 Development of the relative Raman peak intensities of PTB7:PCBM thin films during laser (785 nm) illumination. From top to bottom the different samples with solvent additive dried at 60 °C (A), with solvent additive dried at 150 °C (B) and without solvent additive (C) are displayed. A multiple Lorentzian fit is used and peak areas are normalized to 100% irrespective of the absolute intensities for each point in time.

illumination in ambient atmosphere that has been reported before. This effect is most pronounced in Figure 12A, which shows the solvent additive sample, dried at 60 °C. For the solvent additive sample, which is dried at higher temperature (Figure 12B) and the sample without solvent additive (Figure 12C) the relative decrease of the 1490 cm^{-1} peak is less distinct and sets in after about 30 min. This observation indicates that the stability of the conjugated system in the PTB7:PCBM blend film, which is essential for the application as active layer, is critically dependent on a complete removal of solvent additive molecules during the fabrication process.

As noted above, the Raman peak at 1490 cm^{-1} is a good indicator for the conjugated system, since it represents C═C stretching vibrations in the PTB7 backbone. A shift of this peak toward larger Raman shifts has been reported before and is seen as a measure for the degradation of the PTB7 conjugated polymer network.[38] This shift is also found in the present study and is shown in Figure 13. The low temperature dried, solvent additive free sample shown in blue, features the largest peak shift of more than 3 cm^{-1} within 120 min of illumination, where the shift is more rapid in the initial phase. Qualitatively similar, but with less absolute peak position shift are observed for the solvent additive sample, dried at 150 °C and the sample that was produced without solvent additive, represented by the red and black symbols, respectively. The properly dried sample with solvent additive shows even slightly higher stability in terms of peak position, compared to the neat PTB7:PCBM film.

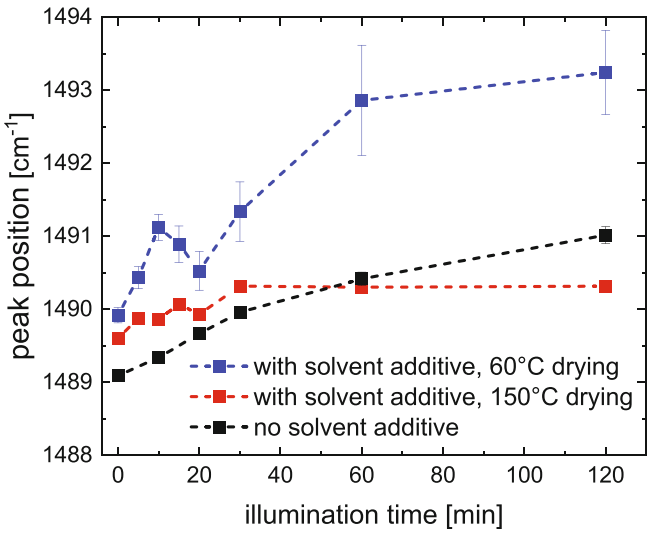

FIGURE 13 Evolution of peak position of the most prominent PTB7 Raman peak at around 1490 cm^{-1} during laser (785 nm) illumination. Respective peak positions are displayed for the different samples with solvent additive dried at 60 °C (blue), with solvent additive dried at 150 °C (red) and without solvent additive (black). The peak is fitted with a single Lorentzian function.

The results from Raman spectroscopy further confirm the trends, which are already shown in our UV–vis and FTIR spectroscopy data. The addition of solvent additive molecules to the polymer:fullerene blend lead to a rapid degradation of the resulting layer. Thus, a complete removal of these additives is absolutely critical in order to fabricate viable and durable devices.

3 | CONCLUSION

The present analysis of UV–vis, FTIR and Raman spectroscopy data during illumination shows the influence of the binary solvent additive DIO:DPE and the applied drying protocol on the stability of PTB7:PCBM films. All methods come to the consistent result that the use of DIO in combination with DPE as solvent additives requires an adapted drying procedure due to their higher boiling point and tendency to remain in the film. The conjugated system in the PTB7:PCBM blend, which is the key for the application in organic photovoltaics, is much more unstable when DIO and DPE are used as solvent additives and the drying temperature is reduced to 60 °C (or 70 °C for the UV–vis analysis). In comparison drying at 150 °C and also a production without solvent additives leads to physically and chemically more stable films. Residual solvent additive molecules are likely to cause this effect since they can act as additional oxidizing agents and are very mobile inside the film, thus providing pathways for material transport (e.g., atmospheric oxygen). Both aspects can be assumed to foster an accelerated degradation. The high diffusivity of DIO in this system has already been shown by quasi-elastic neutron scattering and can be assumed to also hold for the binary system, which is investigated here.[59] The findings emphasize the importance of complete drying of the active layer before its use in a solar cell and reveal the main working points for light and oxygen induced degradation to be considered in future material development.

4 | EXPERIMENTAL SECTION

4.1 | Sample preparation

The low-bandgap conjugated polymer PTB7 (purity: >99.9%, molecular weight: 10,000–120,000 g/mol, polydispersity: 2.6) and the fullerene PCBM (purity: >99.9%) were used to prepare thin films with a weight ratio of 1:1.5, respectively. This blend ratio was reported to be the optimal composition for the application in solar cells but

also for slightly modified systems.[62,68–70] Chlorobenzene (CB) was used as the bulk solvent for both components and for the samples produced with binary solvent additive, diiodooctane (DIO) and diphenylether (DPE) were added to the blend solution. All chemicals were used as purchased from 1-Material (PTB7), Solenne BV (PCBM) and Merck (solvents). For the production of thin films both, PTB7 and PCBM were dissolved in CB (20 mg/mL). To achieve a weight ratio of 1 to 1.5 between PTB7 and PCBM, the solutions were subsequently mixed in a volume ratio of 1:1.5 (PTB7 solution: PCBM solution). For the samples with solvent additive, DIO (3 vol%) and DPE (2 vol%) were added, where the respective fractions refer to the final solution volume. All solutions were stirred for at least 12 h at 70 °C to ensure complete and homogeneous solvation. The final films were produced by drop casting on glass or silicon substrates. The substrates were inclined with an angle of about 20° against horizontal and the respective amount of solution was applied homogeneously with a syringe. Subsequently, the samples were dried on a heating plate at their individual temperature for 10 min. All samples, irrespective of their drying temperature, appeared completely dry and no liquid like or viscous behavior could be observed.

4.2 | X-ray diffraction

Structural investigation of the samples was performed by X-ray diffraction (XRD). A Bruker D8 Advance Laboratory diffractometer with a copper X-ray tube (K-alpha lines at a wavelength of 1.5418 Å) was used. Diffractograms were obtained in a 2-theta range from 3 to 30° with an increment of 0.025° and a measurement time of 3 s per step. Samples were taken out of the diffractometer for the illumination with the blue LED.

4.3 | UV–vis absorption spectroscopy

UV–visible (UV–vis) absorbance spectra were acquired with a Perkin Elmer Lambda 35 spectrometer, in transmission geometry. The wavelength range of the measurement was 350 to 1000 nm using a tungsten halogen lamp. The spectral resolution was 1 nm at a scan speed of 480 nm/min. All samples for UV–vis spectroscopy were drop cast on glass substrates. The amount of solution and subsequent film thickness was chosen to yield maximum absorbance values of 1.0–1.5, according to the Lambert-Beer-Law, in the relevant wavelength range. Samples were fixed to a static sample holder that could be located at the exact same position for each measurement. LED illumination was then performed outside of the spectrometer for the required time before the sample was transferred back into the instrument for the next measurement. Details on the illumination setup and used LED can be found in the supporting information.

4.4 | FTIR spectroscopy

Fourier transformed infrared (FTIR) absorbance measurements were performed with a Bruker Equinox 55 FTIR-spectrometer. Data acquisition and baseline subtraction were performed with the OPUS 6 software. 125 scans from 4000 to 400 cm^{-1} were performed for each measurement with a resolution of approximately 1 cm^{-1} at an acquisition time of 1 s per measurement point. The samples for FTIR-analysis were drop cast on quadratic 20×20 mm^2 silicon substrates with 30 µL solution. Subsequently the sample was fixed to the sample holder and oriented in a 45° angle against the probe light path to allow 90° LED illumination inside the instrument.

4.5 | Raman spectroscopy

Raman spectra were recorded with a modular, fiber-based Raman system, designed by Horiba Yobin. A Horiba iHR 320 spectrometer is used in the system, which was installed in a darkened and temperature controlled environment. A 100 mW infrared laser with a central wavelength of 785 nm was used for excitation. The excitation light was guided through a superhead, where laser and Raman scattering paths are merged and divided, respectively. The light paths traveled through a lens system that focused the laser on a spot approximately 110 mm in front of the last lens. The sample position was manually adjusted around this spot to optimize Raman-scattered signal, reaching back to the superhead through the lens system. Samples were produced analogously to FTIR-samples via drop casting on silicon substrates. For the illumination of the sample the Raman-laser itself was used. In order to slow down the degradation to a measurable timescale, the laser was attenuated by a gray filter with an optical density of 1. The acquisition time for single Raman measurements was set to 20 s.

ACKNOWLEDGMENTS

This work was supported by the German Federal Ministry of Education and Research (BMBF) in the framework of project 05K16WO3 and by the Deutsche Forschungsgemeinschaft (DFG, German Research Foundation) under Germany's Excellence Strategy—EXC 2089/1 − 390776260 (e-conversion). The authors thank the Heinz

Maier-Leibnitz Zentrum (MLZ) and the Forschungs-Neutronenquelle Heinz Maier-Leibnitz (FRM II) for providing the environment for Raman measurements at the instrument TOFTOF. Adrian Stephan helped during the Raman experiments. Open Access funding enabled and organized by Projekt DEAL.

CONFLICT OF INTEREST STATEMENT

The authors declare no conflicts of interest.

ORCID

Peter Müller-Buschbaum https://orcid.org/0000-0002-9566-6088

REFERENCES

[1] X. Wang, Q. Sun, J. Gao, J. Wang, C. Xu, X. Ma, F. Zhang, *Energies* **2021**, *14*, 4200.
[2] F. M. van der Staaij, I. M. van Keulen, E. v. Hauff, *Sol. RRL* **2021**, *5*, 2100167.
[3] M. Giannouli, *Int. J. Photoenergy* **2021**, *2021*, 1.
[4] F. C. Krebs, J. Fyenbo, M. Jørgensen, *J. Mater. Chem.* **2010**, *20*, 8994.
[5] F. C. Krebs, N. Espinosa, M. Hösel, R. R. Søndergaard, M. Jørgensen, *Adv. Mater.* **2014**, *26*, 29.
[6] S. Pröller, F. Liu, C. Zhu, C. Wang, T. P. Russell, A. Hexemer, P. Müller-Buschbaum, E. M. Herzig, *Adv. Energy Mater.* **2016**, *6*, 1501580.
[7] Y. Liu, T. T. Larsen-Olsen, X. Zhao, B. Andreasen, R. R. Søndergaard, M. Helgesen, K. Norrman, M. Jørgensen, F. C. Krebs, X. Zhan, *Sol. Energy Mater. Sol. Cells* **2013**, *112*, 157.
[8] C. N. Hoth, R. Steim, P. Schilinsky, S. A. Choulis, S. F. Tedde, O. Hayden, C. J. Brabec, *Org. Electron.* **2009**, *10*, 587.
[9] R. Green, A. Morfa, A. J. Ferguson, N. Kopidakis, G. Rumbles, S. E. Shaheen, *Appl. Phys. Lett.* **2008**, *92*, 33301.
[10] J. E. Carlé, M. Helgesen, O. Hagemann, M. Hösel, I. M. Heckler, E. Bundgaard, S. A. Gevorgyan, R. R. Søndergaard, M. Jørgensen, R. García-Valverde, S. Chaouki-Almagro, J. A. Villarejo, F. C. Krebs, *Joule* **2017**, *1*, 274.
[11] H. Kang, G. Kim, J. Kim, S. Kwon, H. Kim, K. Lee, *Adv. Mater.* **2016**, *28*, 7821.
[12] Y. Cui, H. Yao, L. Hong, T. Zhang, Y. Tang, B. Lin, K. Xian, B. Gao, C. An, P. Bi, W. Ma, J. Hou, *Natl. Sci. Rev.* **2020**, *7*, 1239.
[13] F. Liu, L. Zhou, W. Liu, Z. Zhou, Q. Yue, W. Zheng, R. Sun, W. Liu, S. Xu, H. Fan, L. Feng, *Adv. Mater.* **2021**, *33*, e2100830.
[14] Y. Lin, Y. Firdaus, F. H. Isikgor, M. I. Nugraha, E. Yengel, G. T. Harrison, R. Hallani, A. El-Labban, H. Faber, C. Ma, X. Zheng, *ACS Energy Lett.* **2020**, *5*, 2935.
[15] C. Li, J. Zhou, J. Song, J. Xu, H. Zhang, X. Zhang, J. Guo, L. Zhu, D. Wei, G. Han, J. Min, Y. Zhang, Z. Xie, Y. Yi, H. Yan, F. Gao, F. Liu, Y. Sun, *Nat. Energy* **2021**, *6*, 605.
[16] P. Bi, S. Zhang, Z. Chen, Y. Xu, Y. Cui, T. Zhang, J. Ren, J. Qin, L. Hong, X. Hao, J. Hou, *Joule* **2021**, *5*, 2408.
[17] Y. Cui, Y. Xu, H. Yao, P. Bi, L. Hong, J. Zhang, Y. Zu, T. Zhang, J. Qin, J. Ren, Z. Chen, *Adv. Mater.* **2021**, *33*, e2102420.
[18] S. Li, C.-Z. Li, M. Shi, H. Chen, *ACS Energy Lett.* **2020**, *5*, 1554.
[19] N. Grossiord, J. M. Kroon, R. Andriessen, P. W. Blom, *Org. Electron.* **2012**, *13*, 432.
[20] J. U. Lee, J. W. Jung, J. W. Jo, W. H. Jo, *J. Mater. Chem.* **2012**, *22*, 24265.
[21] H. Cao, W. He, Y. Mao, X. Lin, K. Ishikawa, J. H. Dickerson, W. P. Hess, *J. Power Sources* **2014**, *264*, 168.
[22] W. Wang, C. J. Schaffer, L. Song, V. Körstgens, S. Pröller, E. D. Indari, T. Wang, A. Abdelsamie, S. Bernstorff, P. Müller-Buschbaum, *J. Mater. Chem. A* **2015**, *3*, 8324.
[23] S. A. Gevorgyan, M. V. Madsen, B. Roth, M. Corazza, M. Hösel, R. R. Søndergaard, M. Jørgensen, F. C. Krebs, *Adv. Energy Mater.* **2016**, *6*, 1501208.
[24] K. S. Wienhold, W. Chen, S. Yin, R. Guo, M. Schwartzkopf, S. V. Roth, P. Müller-Buschbaum, *Sol. RRL* **2020**, *4*, 2000251.
[25] C. J. Schaffer, C. M. Palumbiny, M. A. Niedermeier, C. Burger, G. Santoro, S. V. Roth, P. Müller-Buschbaum, *Adv. Energy Mater.* **2016**, *6*, 1600712.
[26] A. Wadsworth, Z. Hamid, J. Kosco, N. Gasparini, I. McCulloch, *Adv. Mater.* **2020**, *32*, e2001763.
[27] R. Giridharagopal, D. S. Ginger, *J. Phys. Chem. Lett.* **2010**, *1*, 1160.
[28] M. A. Ruderer, P. Müller-Buschbaum, *Soft Matter* **2011**, *7*, 5482.
[29] C. J. Brabec, M. Heeney, I. McCulloch, J. Nelson, *Chem. Soc. Rev.* **2011**, *40*, 1185.
[30] M. C. Scharber, D. Mühlbacher, M. Koppe, P. Denk, C. Waldauf, A. J. Heeger, C. J. Brabec, *Adv. Mater.* **2006**, *18*, 789.
[31] M. C. Scharber, N. S. Sariciftci, *Prog. Polym. Sci.* **2013**, *38*, 1929.
[32] P. Müller-Buschbaum, *Adv. Mater.* **2014**, *26*, 7692.
[33] L. Lu, L. Yu, *Adv. Mater.* **2014**, *26*, 4413.
[34] R. Sharma, H. Lee, V. Gupta, H. Kim, M. Kumar, C. Sharma, S. Chand, S. Yoo, D. Gupta, *Org. Electron.* **2016**, *34*, 111.
[35] D. Bartesaghi, G. Ye, R. C. Chiechi, L. J. A. Koster, *Adv. Energy Mater.* **2016**, *6*, 1502338.
[36] J. Kettle, Z. Ding, M. Horie, G. C. Smith, *Org. Electron.* **2016**, *39*, 222.
[37] Y. W. Soon, H. Cho, J. Low, H. Bronstein, I. McCulloch, J. R. Durrant, *Chem. Commun.* **2013**, *49*, 1291.
[38] J. Razzell-Hollis, J. Wade, W. C. Tsoi, Y. Soon, J. Durrant, J.-S. Kim, *J. Mater. Chem. A* **2014**, *2*, 20189.
[39] S. Shah, R. Biswas, T. Koschny, V. Dalal, *Nanoscale* **2017**, *9*, 8665.
[40] E. Darlatt, B. Muhsin, R. Roesch, C. Lupulescu, F. Roth, M. Kolbe, A. Gottwald, H. Hoppe, M. Richter, *Nanotechnology* **2016**, *27*, 324005.
[41] E. A. Arbab, B. Taleatu, G. T. Mola, *J. Mod. Opt.* **2014**, *61*, 1749.
[42] J. K. Lee, W. L. Ma, C. J. Brabec, J. Yuen, J. S. Moon, J. Y. Kim, K. Lee, G. C. Bazan, A. J. Heeger, *J. Am. Chem. Soc.* **2008**, *130*, 3619.
[43] J. Kniepert, I. Lange, J. Heidbrink, J. Kurpiers, T. J. K. Brenner, L. J. A. Koster, D. Neher, *J. Phys. Chem. C* **2015**, *119*, 8310.
[44] W. Kim, J. K. Kim, E. Kim, T. K. Ahn, D. H. Wang, J. H. Park, *J. Phys. Chem. C* **2015**, *119*, 5954.
[45] S. Guo, E. M. Herzig, A. Naumann, G. Tainter, J. Perlich, P. Müller-Buschbaum, *J. Phys. Chem. B* **2014**, *118*, 344.
[46] M. Ito, K. Palanisamy, A. Kumar, V. S. Murugesan, P.-K. Shin, N. Tsuda, J. Yamada, S. Ochiai, *Int. J. Photoenergy* **2014**, *2014*, 1.

[47] S. B. Dkhil, M. Pfannmöller, M. I. Saba, M. Gaceur, H. Heidari, C. Videlot-Ackermann, O. Margeat, A. Guerrero, J. Bisquert, G. Garcia-Belmonte, A. Mattoni, S. Bals, J. Ackermann, *Adv. Energy Mater.* **2017**, *7*, 1601486.
[48] E. F. Manley, J. Strzalka, T. J. Fauvell, N. E. Jackson, M. J. Leonardi, N. D. Eastham, T. J. Marks, L. X. Chen, *Adv. Mater.* **2017**, *29*, 1703933.
[49] Y. Zheng, G. Wang, D. Huang, J. Kong, T. Goh, W. Huang, J. Yu, A. D. Taylor, *Sol. RRL* **2018**, *2*, 1700144.
[50] B. J. Tremolet de Villers, K. A. O'Hara, D. P. Ostrowski, P. H. Biddle, S. E. Shaheen, M. L. Chabinyc, D. C. Olson, N. Kopidakis, *Chem. Mater.* **2016**, *28*, 876.
[51] A. Tournebize, A. Rivaton, H. Peisert, T. Chassé, *J. Phys. Chem. C* **2015**, *119*, 9142.
[52] L. Ye, Y. Jing, X. Guo, H. Sun, S. Zhang, M. Zhang, L. Huo, J. Hou, *J. Phys. Chem. C* **2013**, *117*, 14920.
[53] H. Waters, N. Bristow, O. Moudam, S.-W. Chang, C.-J. Su, W.-R. Wu, U.-S. Jeng, M. Horie, J. Kettle, *Org. Electron.* **2014**, *15*, 2433.
[54] D. Yang, F. C. Löhrer, V. Körstgens, A. Schreiber, S. Bernstorff, J. M. Buriak, P. Müller-Buschbaum, *ACS Energy Lett.* **2019**, *4*, 464.
[55] I. Fraga Domínguez, P. D. Topham, P.-O. Bussière, D. Bégué, A. Rivaton, *J. Phys. Chem. C* **2015**, *119*, 2166.
[56] A. Rivaton, A. Tournebize, J. Gaume, P.-O. Bussière, J.-L. Gardette, S. Therias, *Polym. Int.* **2014**, *63*, 1335.
[57] G. Griffini, S. Turri, M. Levi, *Polym. Bull.* **2011**, *66*, 211.
[58] F. Liu, W. Zhao, J. R. Tumbleston, C. Wang, Y. Gu, D. Wang, A. L. Briseno, H. Ade, T. P. Russell, *Adv. Energy Mater.* **2014**, *4*, 1301377.
[59] D. M. Schwaiger, W. Lohstroh, P. Müller-Buschbaum, *Macromolecules* **2021**, *54*, 6534.
[60] F. C. Löhrer, C. Senfter, C. J. Schaffer, J. Schlipf, D. Moseguí González, P. Zhang, S. V. Roth, P. Müller-Buschbaum, *Adv. Photonics Res.* **2020**, *1*, 2000047.
[61] M. O. Reese, A. J. Morfa, M. S. White, N. Kopidakis, S. E. Shaheen, G. Rumbles, D. S. Ginley, *Sol. Energy Mater. Sol. Cells* **2008**, *92*, 746.
[62] C. Liu, C. Yi, K. Wang, Y. Yang, R. S. Bhatta, M. Tsige, S. Xiao, X. Gong, *ACS Appl. Mater. Interfaces* **2015**, *7*, 4928.
[63] S. T. Hoffmann, H. Bässler, A. Köhler, *J. Phys. Chem. B* **2010**, *114*, 17037.
[64] K. S. Wienhold, V. Körstgens, S. Grott, X. Jiang, M. Schwartzkopf, S. V. Roth, P. Müller-Buschbaum, *Sol. RRL* **2020**, *4*, 2000086.
[65] S. Kim, M. A. M. Rashid, T. Ko, K. Ahn, Y. Shin, S. Nah, M. H. Kim, B. Kim, K. Kwak, M. Cho, *J. Phys. Chem. C* **2020**, *124*, 2762.
[66] A. Perthué, T. Gorisse, H. Santos Silva, D. Bégué, A. Rivaton, G. Wantz, *Mater. Chem. Front.* **2019**, *3*, 1632.
[67] M. D. Lesoine, J. M. Bobbitt, J. A. Carr, M. Elshobaki, S. Chaudhary, E. A. Smith, *J. Phys. Chem. C* **2014**, *118*, 30229.
[68] V. Pranculis, A. Ruseckas, D. A. Vithanage, G. J. Hedley, I. D. W. Samuel, V. Gulbinas, *J. Phys. Chem. C* **2016**, *120*, 9588.
[69] Z. He, B. Xiao, F. Liu, H. Wu, Y. Yang, S. Xiao, C. Wang, T. P. Russell, Y. Cao, *Nat. Photon* **2015**, *9*, 174.
[70] L. Song, W. Wang, E. Barabino, D. Yang, V. Körstgens, P. Zhang, S. V. Roth, P. Müller-Buschbaum, *ACS Appl. Mater. Interfaces* **2019**, *11*, 3125.

SUPPORTING INFORMATION

Additional supporting information can be found online in the Supporting Information section at the end of this article.

How to cite this article: D. M. Schwaiger, W. Lohstroh, M. Wolf, C. J. Garvey, P. Müller-Buschbaum, *J. Polym. Sci.* **2023**, *61*(15), 1660. https://doi.org/10.1002/pol.20230072